

# Using Small Unmanned Aerial Vehicles for Turbulence Measurements in the Atmosphere<sup>1</sup>

A. P. Shelekhov<sup>a, \*</sup>, A. L. Afanasiev<sup>b</sup>, E. A. Shelekhova<sup>a</sup>, A. A. Kobzev<sup>a</sup>, A. E. Tel'minov<sup>a</sup>,  
A. N. Molchunov<sup>a</sup>, and O. N. Poplevina<sup>a</sup>

<sup>a</sup> *Institute of Monitoring of Climatic and Ecological Systems, Siberian Branch, Russian Academy of Sciences, Tomsk, 634055 Russia*

<sup>b</sup> *Zuev Institute of Atmospheric Optics Organization, Siberian Branch, Russian Academy of Sciences, Tomsk, 634055 Russia*  
*\*e-mail: ash1404@mail.ru*

Received May 17, 2021; revised May 28, 2021; accepted June 9, 2021

**Abstract**—This paper demonstrates the possibility of using the telemetry of small unmanned aerial vehicles (UAVs) to monitor the state of atmospheric turbulence. The turbulence spectrum is determined from data on the roll, pitch, and yaw angles of the DJI Mavic Mini quadcopter and then compared with measurements of AMK-03 autonomous sonic weather station. The measurements are carried out at the Basic Experimental Complex (BEC) of the Zuev Institute of Atmospheric Optics, Siberian Branch, Russian Academy of Sciences (SB RAS) (Tomsk, Russia), the territory of which has a nearly smooth and uniform surface, on July 24 and August 12, 2020. It has been found that the turbulence spectra obtained with AMK-03 and the DJI Mavic Mini are generally identical with minor discrepancies in the high-frequency spectral range from  $f \sim 1$  Hz. For the data obtained in July, the turbulence spectra in the inertial range obey the 5/3 law, and the relation of measured turbulence spectra of the longitudinal and transverse velocity components corresponds to the Kolmogorov–Obukhov isotropic turbulence. As for the data obtained in August, a slight deviation from the 5/3 law was observed in both AMK-03 and DJI Mavic Mini measurements. The longitudinal and transverse turbulence scales were estimated by the least-square fit method with the von Karman model as a regression curve. The turbulence scales calculated from the July and August data of AMK-03 and the DJI Mavic Mini coincide, and the condition describing the relation between the longitudinal and transverse scales in the isotropic atmosphere stays true to a good accuracy.

**Keywords:** unmanned aerial vehicle, low-altitude sounding, atmospheric turbulence, spectrum, turbulence scales

**DOI:** 10.1134/S0001433821050133

## INTRODUCTION

Atmospheric turbulence, which manifests itself in irregular pulsations of the air-flow velocity both in time and in space, has a strong and sometimes catastrophic effect on aircraft. This effect essentially depends on the size and weight of the aircraft. Compared to airplanes and helicopters, the size and weight of unmanned aerial vehicles (UAVs) can be significantly smaller, resulting in a stronger effect of turbulence on the aircraft. Also, UAVs can fly at significantly lower altitudes than manned vehicles. At low altitudes, the underlying surface has an additional effect on the state of atmospheric turbulence, which manifests itself in the appearance of additional turbulent eddies. Thus, the turbulent atmosphere complicates UAV movement to a greater extent, and the pres-

ence of buildings and complex orography in a city additionally impairs navigation in an environment with random pulsations of wind speed. One urgent problem of navigation in a turbulent atmosphere is monitoring and forecasting the state of turbulent vortex formations arising during cargo transportation using UAVs in a smart city at an altitude range of up to 500 m [1].

It is known [2] that, in order to describe the state of a UAV, in addition to knowing the speed of the vehicle relative to the air mass, information about the turbulence spectrum along its path in a turbulent atmosphere is required. The results of experimental studies show that a good approximation for describing the state of a UAV is an approach based on the transmission of white noise through a linear filter specified by the Karman turbulence spectrum. In addition to the Karman spectrum, a suitable approximation for problems of UAV dynamics in a turbulent atmosphere is the Dryden turbulence model [2]; other models, for

<sup>1</sup> The paper was prepared based on an oral report presented at the All-Russia Conference on Turbulence, Dynamics of Atmosphere and Climate dedicated to the memory of Academician A.M. Obukhov (Moscow, November 10–12, 2020).

example, the unified turbulence model [3], can also be used. Thus, monitoring and forecasting the state of vortex formations is reduced to determining the spectrum of turbulence along the route of a UAV in a smart city.

Sodars, lidars, and radars effective means of remote sensing a turbulent atmosphere, and acoustic anemometers are the most popular contact monitoring method. In recent years, small UAVs have also become a popular tool in the field of atmospheric monitoring. The most urgent problem in this area is the use of UAVs for the low-altitude sounding of the atmosphere in hard-to-reach places and in areas with complex orography, such as the Arctic region, urban environment, and mountainous terrain. In [4, 5], various aspects of the use of UAVs for studying the atmospheric boundary layer and the prospects for the use of unmanned aerial vehicles in meteorology and atmospheric physics are considered.

The main trend in this area is diagnostics of the speed of movement of the flow of air masses [6–10]. In addition to the wind speed, it is of interest to study the fluctuation characteristics of a turbulent atmosphere. At the beginning, low-altitude sounding of the fluctuation characteristics of the turbulent atmosphere was carried out using a fixed-wing UAV [11–16]. These works show the fundamental possibility of measuring turbulence spectra using fixed-wing UAVs of various sizes and weights. In the process of sounding, a UAV of this type moves in space for a long time in order to obtain a representative series of observations of wind speed fluctuations. As a result of such a sensing scheme, there is an uncertainty in space when measuring the turbulence spectrum. This kind of uncertainty can be eliminated by using multirotor UAVs, which are able to hover at a fixed point in space for a long time.

It is shown in [17–19] that the use of a quadcopter in the altitude hold mode allows one to obtain the course of the turbulence spectrum, which coincides with the measurements obtained using acoustic anemometry. This coincidence suggests that a quadcopter can be used to study the spectrum of turbulence and its characteristics, for example, energy and inertial ranges and the integral scale of turbulence, and, therefore, monitor and predict the state of the turbulent atmosphere during cargo transportation using UAVs in a smart city.

This paper presents the results of measuring the turbulence spectra and integral scales obtained using a DJI Mavic Mini quadcopter and the AMK-03 automated meteorological complex. Experimental studies were carried out at the Basic Experimental Complex of the Zuev Institute, SB RAS (BEC), the surface of which is close to flat and homogeneous.

## 1. LONGITUDINAL AND TRANSVERSE TURBULENCE SPECTRUM

In the coordinate system, in which one of the axes is directed along the average wind speed, the velocity field of the turbulent air flow has the form [20, 21]

$$u(r, 0, 0; t) = \langle u \rangle + u'(r, 0, 0; t), \quad (1)$$

$$v = v'(r, 0, 0; t), \quad (2)$$

$$w = w'(r, 0, 0; t), \quad (3)$$

where  $\langle u \rangle$  is average wind speed;  $u'$ ,  $v'$ , and  $w'$  are fluctuations in the air wind speed; and  $\langle \dots \rangle$  is the operator of statistical averaging.

The main advantage of the coordinate system, in which one of the axes is directed in the direction of the mean wind speed, is the possibility of using Taylor's hypothesis about the "frozenness" of turbulent fluctuations [20, 21]. The essence of this hypothesis is that the entire spatial turbulent picture moves in time with an average wind speed  $\langle u \rangle$ . As a result, we obtain a simple theoretical relationship between the spatiotemporal and purely spatial characteristics of the fluctuations of the wind speed field,

$$u'(r, 0, 0; t) = u'(r - \langle u \rangle t, 0, 0), \quad (4)$$

$$v'(r, 0, 0; t) = v'(r - \langle u \rangle t, 0, 0), \quad (5)$$

$$w'(r, 0, 0; t) = w'(r - \langle u \rangle t, 0, 0), \quad (6)$$

which allows us to compare the behavior of the temporal spectra measured experimentally with theoretical results.

One of the most frequently used models of turbulence spectra is the Karman model [3, 20, 21], which allows one to study the behavior of the spectrum in the energy and inertial ranges. Expressions for the longitudinal and transverse time spectra of turbulence for the Karman model have the form

$$\frac{\Phi_u(f)}{\sigma_u^2} = \frac{2L_u}{\pi} \frac{1}{\left[1 + (1.339L_u 2\pi f / \langle u \rangle)^2\right]^{5/6}}, \quad (7)$$

$$\frac{\Phi_v(f)}{\sigma_v^2} = \frac{2L_v}{\pi} \frac{1 + 8/3(2.678L_v 2\pi f / \langle w \rangle)^2}{\left[1 + (2.678L_v 2\pi f / \langle u \rangle)^2\right]^{11/6}}, \quad (8)$$

where  $L_u$  is the longitudinal scale of turbulence,  $L_v$  is the transverse scale of turbulence,  $\sigma_u^2$  and  $\sigma_v^2$  is the dispersion of the longitudinal and transverse components of the wind speed. In the case of an isotropic atmosphere, we have the following expression for these scales:

$$L_v = L_u/2. \quad (9)$$

In the inertial range for isotropic turbulence, the turbulence spectrum of longitudinal and transverse

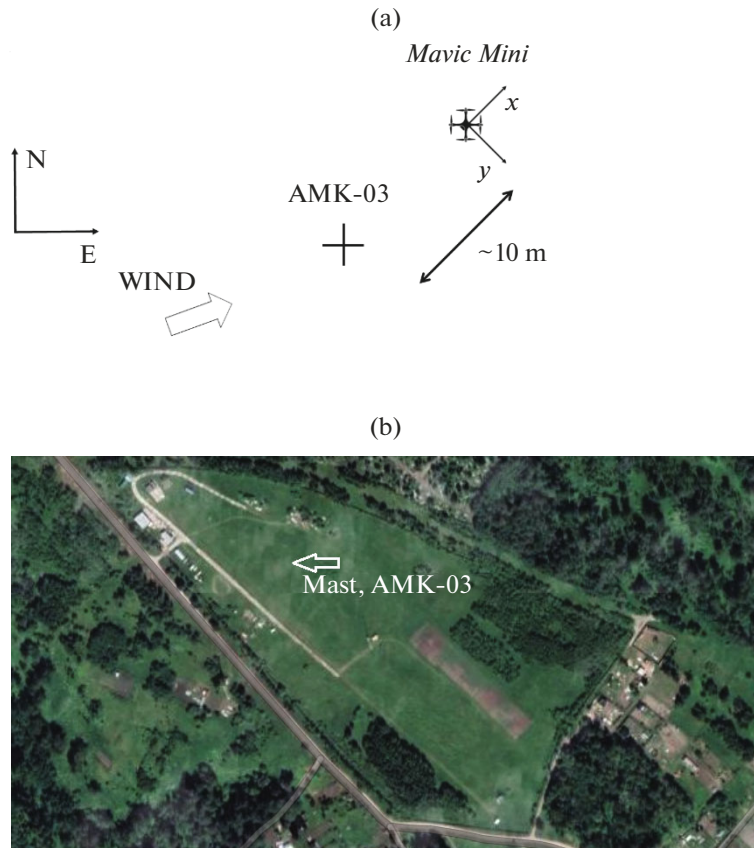


**Fig. 1.** Experiment scheme (a) and Google map of the area of the Basic Experimental Complex of the Zuev Institute of Atmospheric Optics Organization, SB RAS (b).

velocity fluctuations obeys the Kolmogorov–Obukhov 5/3 law [3, 20, 21],

$$\frac{\Phi_u(f)}{\sigma_u^2} \sim f^{-5/3}, \tag{10}$$

$$\frac{\Phi_v(f)}{\sigma_v^2} \sim f^{-5/3}, \tag{11}$$

and the relationship between the turbulence spectra of longitudinal and transverse velocity fluctuations has the form

$$\frac{4}{3} \frac{\Phi_u(f)}{\sigma_u^2} = \frac{\Phi_v(f)}{\sigma_v^2}. \tag{12}$$

## 2. LONGITUDINAL AND TRANSVERSE VELOCITY FLUCTUATIONS

Figure 1a schematically shows the arrangement of the instruments and the direction of the average wind speed during the experiments. It can be seen that, when making measurements, the use of a coordinate system in which one of the axes is directed along the average wind speed is fraught with significant difficulties. For a correct comparison of experimental data

with theoretical results, an approach is used that excludes the accurate positioning of instruments in the direction of the mean wind.

It is well known that in the atmosphere there is often a case where the horizontal transfer of air masses prevails over the vertical movement; therefore, we will direct one of the axes of the coordinate system considered in the previous section along the mean horizontal wind. When carrying out measurements, the automated meteorological complex AMK-03 was oriented to the cardinal points and the quadcopter was randomly oriented. In this case, the longitudinal and transverse turbulent fluctuations of the wind speed will take the form

$$u' = n_E w'_E + n_N w'_N, \tag{13}$$

$$v' = -n_N w'_E + n_E w'_N, \tag{14}$$

$$\mathbf{n} = \{n_E, n_N, 0\} = \left\{ \frac{\langle w_E \rangle}{\langle u \rangle}, \frac{\langle w_N \rangle}{\langle u \rangle}, 0 \right\} \tag{15}$$

for AMK-03 and

$$u' = n_x w'_x + n_y w'_y, \tag{16}$$

$$v' = -n_x w'_y + n_y w'_x, \tag{17}$$

$$\mathbf{n} = \{n_x, n_y, 0\} = \left\{ \frac{\langle w_x \rangle}{\langle u \rangle}, \frac{\langle w_y \rangle}{\langle u \rangle}, 0 \right\} \quad (18)$$

for a quadcopter. Here,  $w'_E$  and  $w'_N$  are fluctuations of the wind-speed components along axes  $E$  and  $N$  according to AMK-03,  $w'_x$  and  $w'_y$  are estimates of fluctuations of the wind-speed components obtained on the basis of the results of quadcopter telemetry,  $\langle w_E \rangle$  and  $\langle w_N \rangle$  are average components of the horizontal velocity along the axes  $E$  and  $N$ , and  $\langle w_x \rangle$  and  $\langle w_y \rangle$  are estimates of the velocity components along the axes  $x$  and  $y$ .

### 3. ESTIMATES OF WIND-SPEED COMPONENTS

In a turbulent atmosphere, the roll, pitch, and yaw angles are the sum of the mean and fluctuation components:  $\varphi = \langle \varphi \rangle + \varphi'$ ,  $\theta = \langle \theta \rangle + \theta'$ , and  $\psi = \langle \psi \rangle + \psi'$ . It is shown in [17–19] that, for ideal hovering, the equations for estimating the wind-speed components obtained on the basis of the results of quadcopter telemetry can be written as the sum of the regular and fluctuation parts

$$w_x = -\frac{mg}{c_x} (\langle \varphi \rangle s_{\langle \psi \rangle} + \langle \theta \rangle c_{\langle \psi \rangle}) - \frac{mg}{c_x} (\varphi' s_{\langle \psi \rangle} + \theta' c_{\langle \psi \rangle}), \quad (19)$$

$$w_y = -\frac{mg}{c_y} (-\langle \varphi \rangle c_{\langle \psi \rangle} + \langle \theta \rangle s_{\langle \psi \rangle}) - \frac{mg}{c_y} (-\varphi' c_{\langle \psi \rangle} + \theta' s_{\langle \psi \rangle}) \quad (20)$$

in the linear case and

$$w_x = -\text{sgn}(\langle \varphi \rangle s_{\langle \psi \rangle} + \langle \theta \rangle c_{\langle \psi \rangle}) \times \sqrt{\frac{2mg}{\rho C_x A_x}} |(\langle \varphi \rangle s_{\langle \psi \rangle} + \langle \theta \rangle c_{\langle \psi \rangle})| \times \left\{ 1 + \frac{\varphi' s_{\langle \psi \rangle} + \theta' c_{\langle \psi \rangle}}{2(\langle \varphi \rangle s_{\langle \psi \rangle} + \langle \theta \rangle c_{\langle \psi \rangle})} \right\}, \quad (21)$$

$$w_y = -\text{sgn}(-\langle \varphi \rangle c_{\langle \psi \rangle} + \langle \theta \rangle s_{\langle \psi \rangle}) \times \sqrt{\frac{2mg}{\rho C_x A_x}} |(-\langle \varphi \rangle c_{\langle \psi \rangle} + \langle \theta \rangle s_{\langle \psi \rangle})| \times \left\{ 1 + \frac{-\varphi' c_{\langle \psi \rangle} + \theta' s_{\langle \psi \rangle}}{2(-\langle \varphi \rangle c_{\langle \psi \rangle} + \langle \theta \rangle s_{\langle \psi \rangle})} \right\} \quad (22)$$

in the quadratic case. Here  $c_j$  and  $C_j$  are resistance coefficients along the axes  $x$  and  $y$ ,  $m$  is the mass of the quadcopter,  $g$  is the acceleration of gravity,  $\rho$  is air density,  $A_j$  are projections of the quadcopter area along axes  $x$  and  $y$ , and  $\text{sgn}(\bullet)$  is the sign function.

It can be seen from expressions (19)–(22) that the estimates of fluctuations of the wind-speed compo-

nents are directly proportional to the fluctuations of the roll and pitch angles. Consequently, the telemetry data of the quadcopter can be used to measure the estimation of fluctuations of the wind-speed components and formulas (16)–(18) allow us to calculate the turbulence spectrum. Formulas (13)–(15) can be used to calculate the turbulence spectra from AMK-03 data, which are objective information about the state of atmospheric turbulence. As a result of these calculations, it is possible to compare the turbulence spectra according to the AMK-03 data and the telemetry data of the quadcopter.

### 4. EXPERIMENT OVERVIEW

Experimental studies were carried out at the Basic Experimental Complex of the Zuev Institute, SB RAS (BEC), July 24 and August 12, 2020. Figure 1b shows a Google map of the BEC area; the arrow shows the location of the meteorological mast on which two AMK-03s are installed at different heights. The terrain on which the BEC is located is not, in the strict sense, a flat and uniform surface. The surface of the ground has a slight slope; on one side it borders a cottage village and there is a forest at the border of the other side. When conducting experiments on such a territory, deviations from isotropic turbulence are possible. In the June experiment, the start time of the research was 05:01 UTC it ended at 05:24 UTC; for the measurements in August, flights were carried out from 06:44 UTC to 07:07 UTC. The start point of the DJI Mavic Mini quadcopter was in the immediate vicinity of a 30-m meteorological mast.

Figure 2 shows the flight paths of the quadcopter during the experiments. After takeoff, the UAV climbed to heights of 10 and 27 m, respectively, for July 24 and August 12, and flew up to AMK-03 [22, 23], located on the mast. The quadcopter was in the altitude hold mode near AMK-03 for more than 20 min, after which it returned to the starting point. Wind data were recorded by AMK-03 at a frequency of 80 Hz, and the data on the state of the quadcopter was recorded at a frequency of 10 Hz.

According to the Tomsk International Airport, which is located ~10 km from the BEC, during the experiment on July 24, 2020, good weather conditions were observed in terms of the quadcopter flight: southwestern wind, speed 1.0 m/s, air temperature 21°C, air humidity 51%, and no precipitation. Good weather conditions were also recorded on August 12: south-southwest wind, speed 4–5 m/s, air temperature 28°C, air humidity 48%, and no precipitation. During the experiment on July 24, according to AMK-03 data on the BEC, the average wind speed at a height of 10 m was 1.25 m/s and, on August 12, at a height of 27 m, 2.6 m/s (at times the wind speed increased to 5 m/s and more).

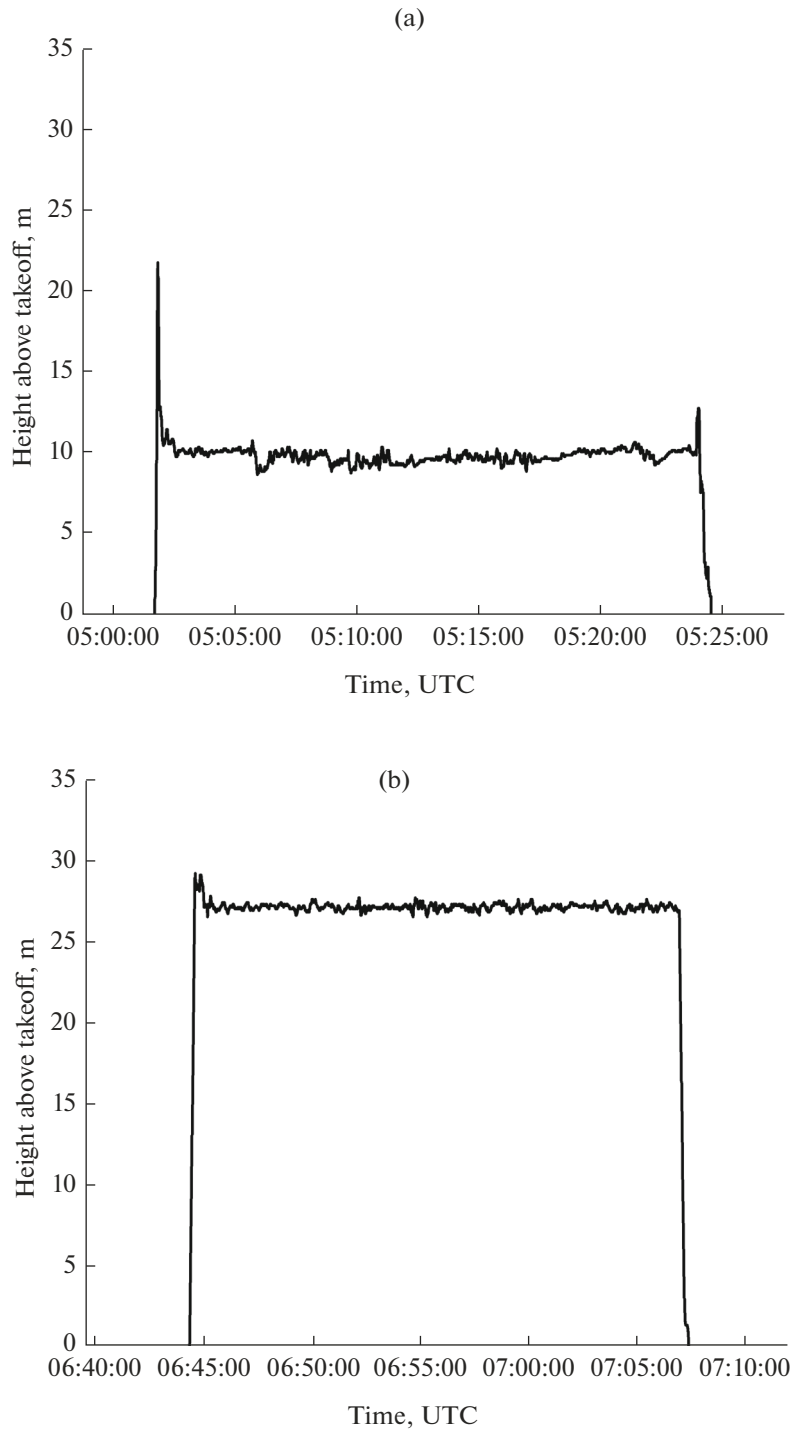
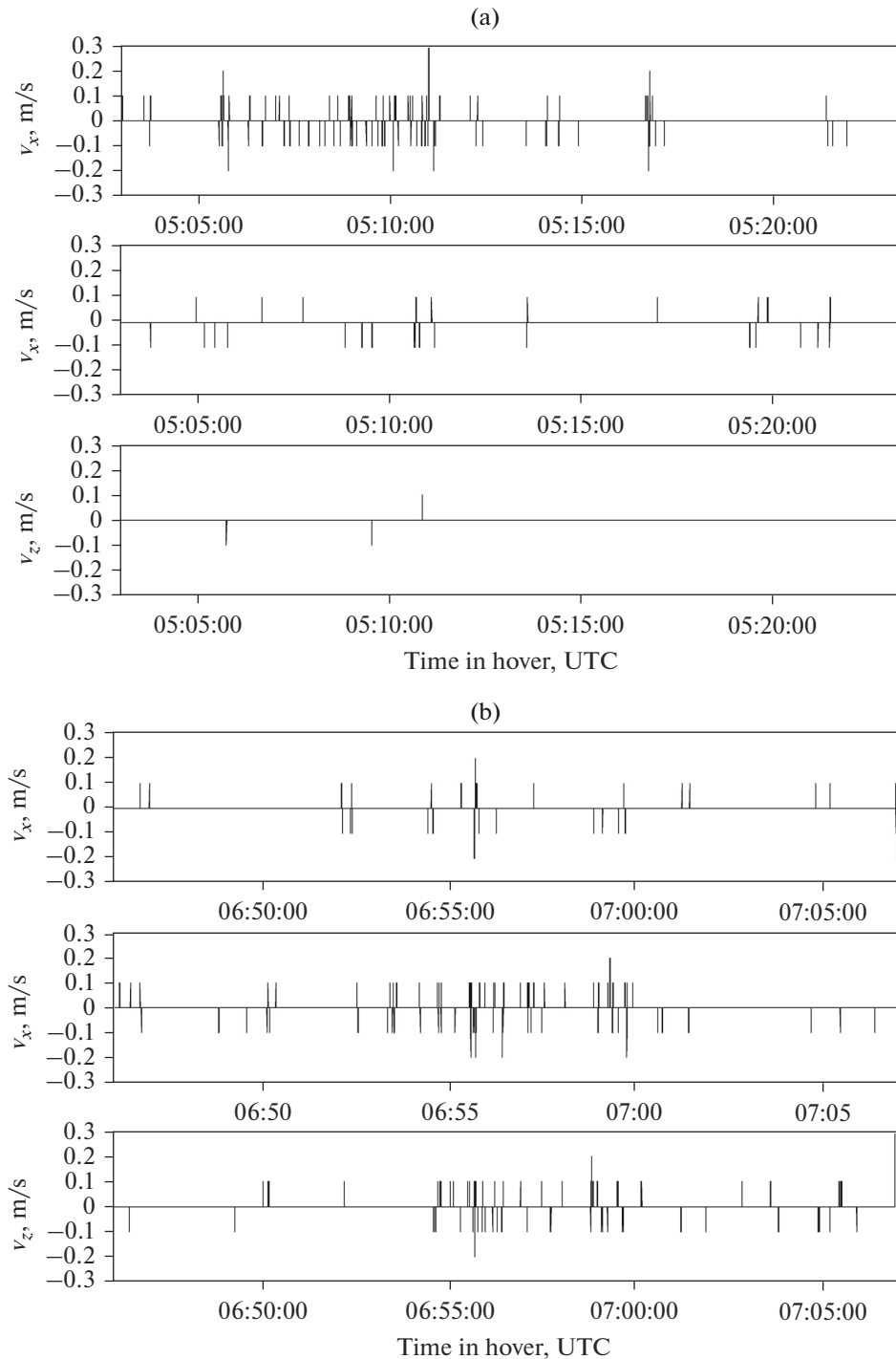


Fig. 2. Flight path of the DJI Mavic Mini quadcopter during the experiment; July 24 (a) and August 12, 2020 (b).

Figure 3 shows changes in the speed components of the quadcopter relative to the Earth along the axes  $x$ ,  $y$ , and  $z$  while hovering: July 24 (a) and August 12, 2020 (b). It can be seen that, in general, when making measurements, the speed components of the quadcopter are equal to zero. In short periods of time, the forces acting on the UAV exceed the capabilities of the control

system and high-precision positioning is disrupted. After regaining control, the quadcopter begins to move to its original position and, upon reaching which, it stops. Thus, the periods at which the positioning of the quadcopter in space is violated can be neglected due to their insignificance and we can assume that ideal hovering was observed during the experiments.



**Fig. 3.** Quadcopter speed components of the DJI Mavic Mini relative to the Earth along axes  $x$ ,  $y$ , and  $z$  during the hovering period, July 24 (a) and August 12, 2020 (b).

Let us consider the behavior of the estimates of the longitudinal and transverse components of the wind speed according to the quadcopter data in the mode of keeping altitude in a turbulent atmosphere and compare it with the measurement results obtained with the AMK-03. To visually compare the measurements of the longitudinal and transverse components of the

wind speed, which were obtained by two methods, we used a phenomenological approach based on the experimental relationship between these components and the angles of roll, pitch, and yaw. This approach allows us to avoid precisely determining the resistance and area coefficients, which are difficult to determine experimentally. The main formulas of the approach

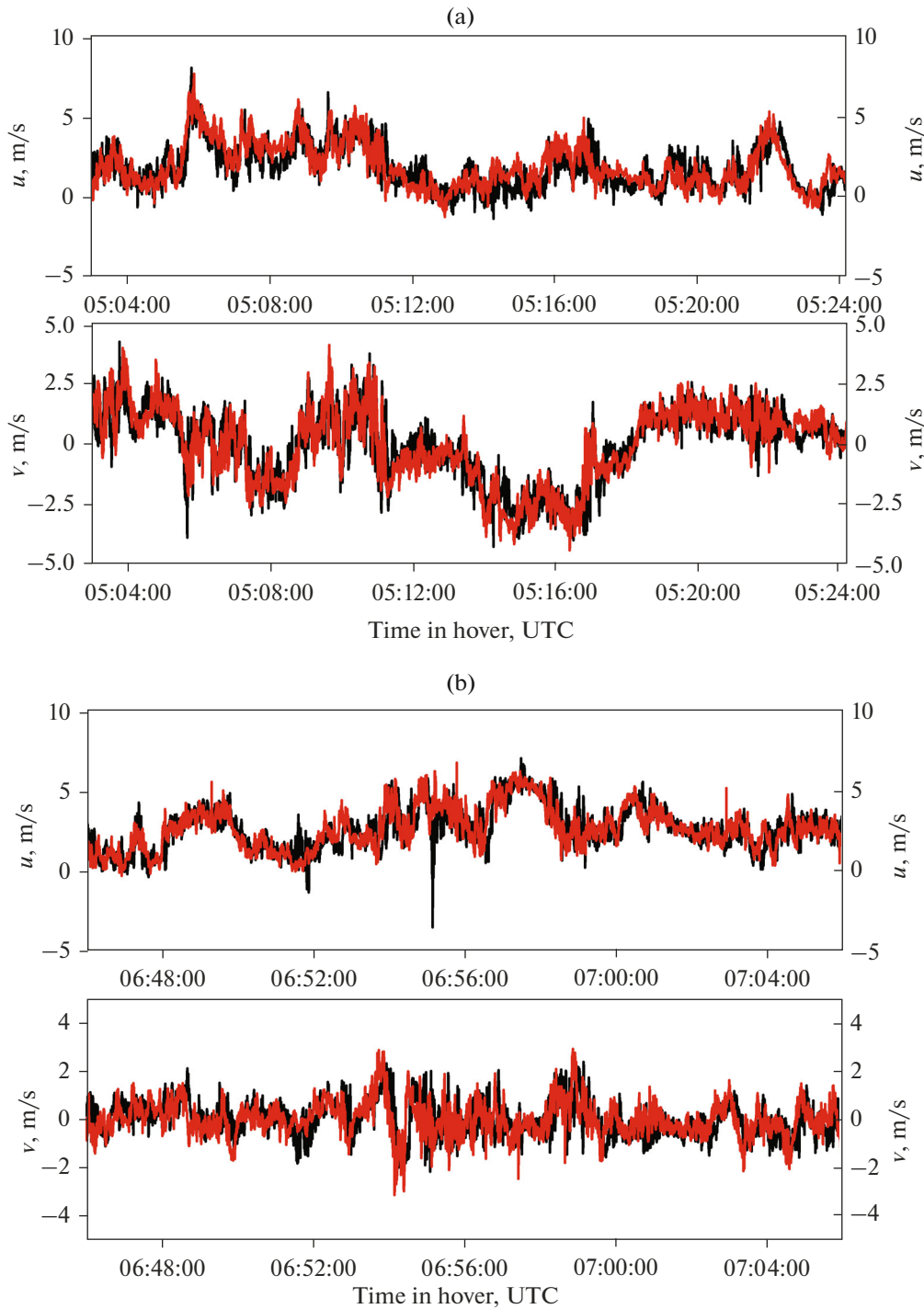


**Fig. 4.** Temporal changes in the longitudinal and transverse components of the wind speed, measured with AMK-03 (red curves) and the DJI Mavic Mini (black curves) on July 24 (a) and August 12, 2020 (b).

and the values of the coefficients obtained phenomenologically are presented in the Appendix. Note that this approach is used by us only for a visual comparison of measurements of the longitudinal and transverse components of the wind speed, which were obtained using AMK-03 and the DJI Mavic Mini. When examining relative turbulence spectra and deter-

mining the scale of turbulence, it is not necessary to follow the procedure outlined in the Appendix.

Figure 4 shows the results of temporal changes in the longitudinal and transverse components of the wind speed measured using AMK-03 (red curves) and the DJI Mavic Mini (black curves): July 24 (a) and

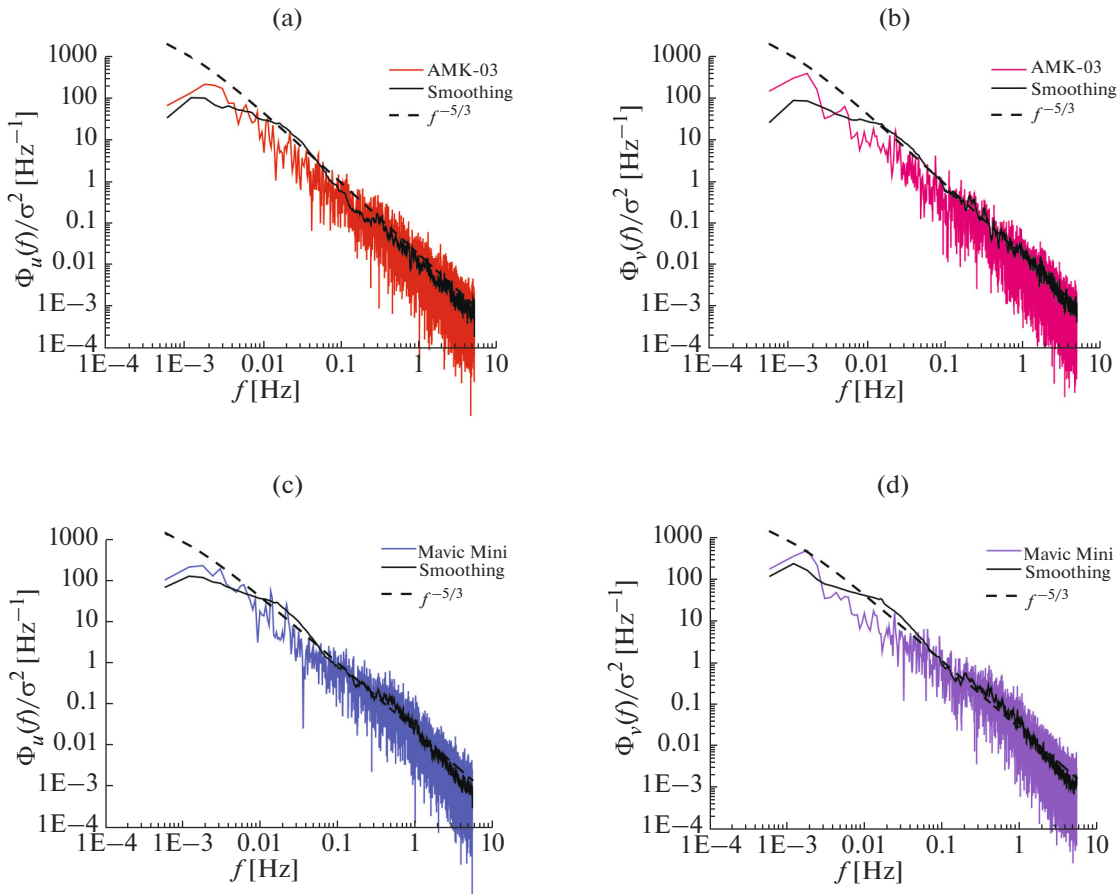


**Fig. 5.** Results of measurements of turbulence spectra on July 24, 2020. Longitudinal and transverse spectra  $\Phi_u(f)$  and  $\Phi_v(f)$ , calculated according to AMK-03 data (a, b) and according to DJI Mavic Mini data (c, d);  $\sigma^2$  is the normalization factor.

August 12, 2020 (b). From Fig. 4 it follows that time series  $u$  and  $v$  measured in different ways are the same; the differences are observed in the high-frequency region of fluctuations.

Figures 5 and 6 show the results of calculations of relative turbulence spectra obtained on the basis of data from AMK-03 (Figs. 5a, 5b, 6a, 6b) and a DJI Mavic Mini quadcopter (Figs. 5c, 5d, 6c, 6d);  $\sigma^2$  is the normalization factor. In the figures, the red and blue curves indicate the turbulence spectra of the longitudinal velocity component; the pink and purple curves show the turbulence spectra of the transverse velocity component, respectively. It can be seen that the values of the spectra change significantly with insignificant changes in frequency. These changes are random oscillations around the main regularities of the turbulence spectra. In order to explicitly see these regularities in the turbulence spectra, a smoothing procedure was used. The result of applying the smoothing procedure is shown in Figs. 5 and 6 by solid black curves.

In Figs. 5 and 6, it can be seen that the turbulence spectra obtained with AMK-03 and the DJI Mavic

Mini, on the whole, coincide and insignificant differences are observed in the high-frequency region of the spectrum, starting from  $f \sim 1$  Hz. In the high-frequency region, the turbulence spectrum for the DJI Mavic Mini attenuates insignificantly with increasing frequency, but faster than in the case of data obtained using AMK-03.

It is well known [20, 21] that the turbulence spectrum has three main spectral regions—the energy range which contains the main part of turbulent energy and where the energy is generated by buoyancy and shear; the inertial range in which energy is not generated or dissipated, but is transmitted from large to smaller scales; and the range of dissipation in which kinetic energy is converted into internal energy. Let us consider the behavior of the turbulence spectra in the inertial and energy ranges.

The behavior of the turbulence spectra of longitudinal and transverse velocity fluctuations in the inertial range obeys the Kolmogorov–Obukhov 5/3 law and is described by formulas (10) and (11). The dotted curves in Figs. 5 and 6 show the spectra  $\Phi(f) \sim f^{-5/3}$ ,



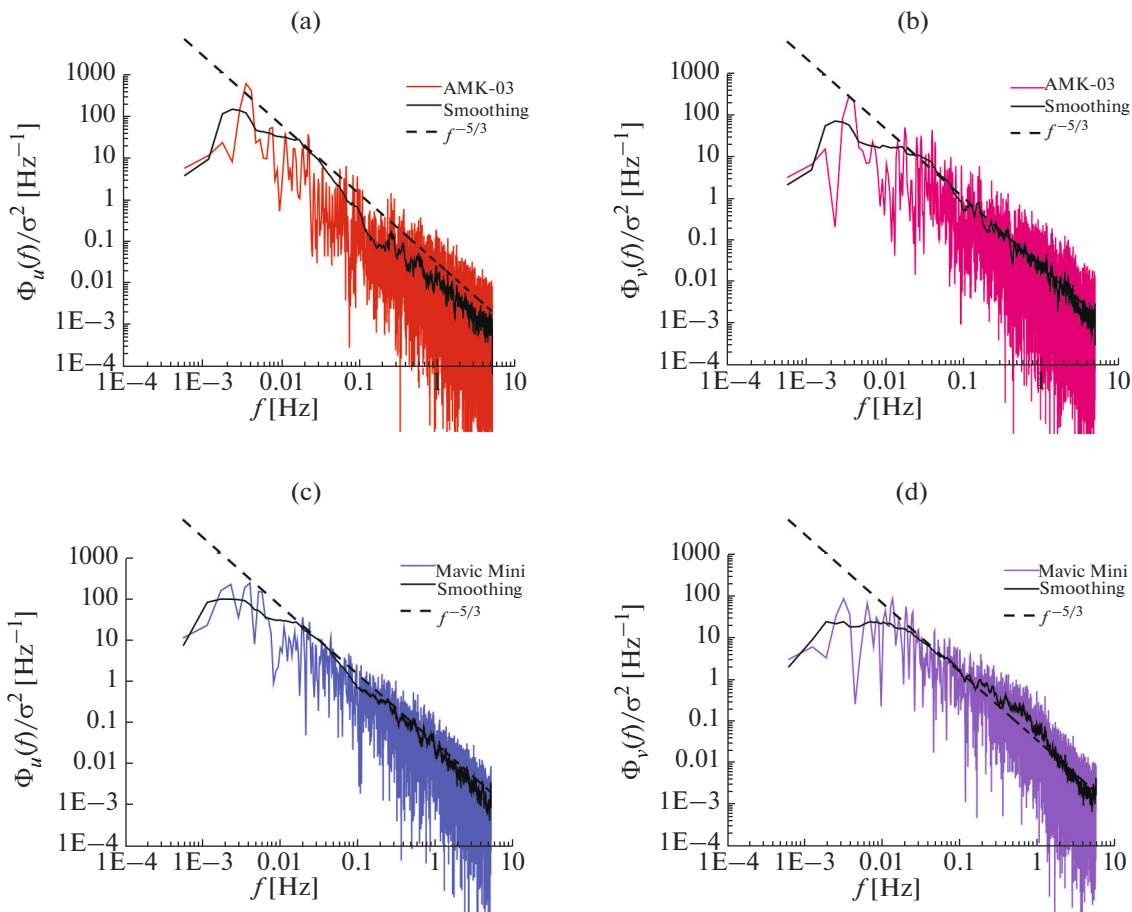


**Fig. 6.** Results of measurements of turbulence spectra on August 12, 2020. Longitudinal and transverse spectra  $\Phi_u(f)$  and  $\Phi_v(f)$  calculated according to AMK-03 data (a, b) and according to DJI Mavic Mini data (c, d);  $\sigma^2$  is the normalization factor.

which corresponds to the Kolmogorov–Obukhov 5/3 law. These figures demonstrate the fact that, during the experiment, Kolmogorov turbulence was observed in the inertial range and this law is qualitatively fulfilled in a wide frequency range.

From formula (12) it follows that in the inertial range for isotropic turbulence  $\sigma_u^2 = \sigma_v^2$ , so the ratio of the turbulence spectra  $K_{4/3} = \Phi_v(f)/\Phi_u(f) = 4/3 \approx 1.33$ . Figure 7 shows the results of a comparison of the turbulence spectra for the longitudinal and transverse velocity components. It can be seen that, for measurements obtained on July 24, 2020, in the same frequency range,  $f \in [0.035, 0.065]$ , spectrum curve  $\Phi_u(f)$  lies below the curve  $\Phi_v(f)$  as for AMK-03 and the DJI Mavic Mini. In the case of measurements carried out on August 12, 2020, the longitudinal spectrum curve also lies below the transverse component spectrum curve, but in different frequency ranges:  $f \in [0.041, 0.011]$  for AMK-03 and  $f \in [0.064, 0.011]$  for a quadcopter.

Average coefficient values  $K_{4/3}$  are given in Table 1. It is seen that the average value of the coefficient  $K_{4/3}$  for measurements obtained on July 24, 2020, in the frequency range  $f \in [0.035, 0.065]$  coincides with its value for isotropic turbulence. There is also good agreement between the values of the coefficient  $K_{4/3}$  between AMK-03 data and the DJI Mavic Mini.

It also follows from the data given in Table 1 that insignificant anisotropy of turbulence was observed on August 12, 2020. Average odds  $K_{4/3}$  for measurements

**Table 1.** Average coefficient values  $\langle K_{4/3} \rangle$

	AMK-03	DJI Mavic Mini
July 24, 2020		
$\langle K_{4/3} \rangle$	1.23	1.22
August 12, 2020		
$\langle K_{4/3} \rangle$	2.02	1.81

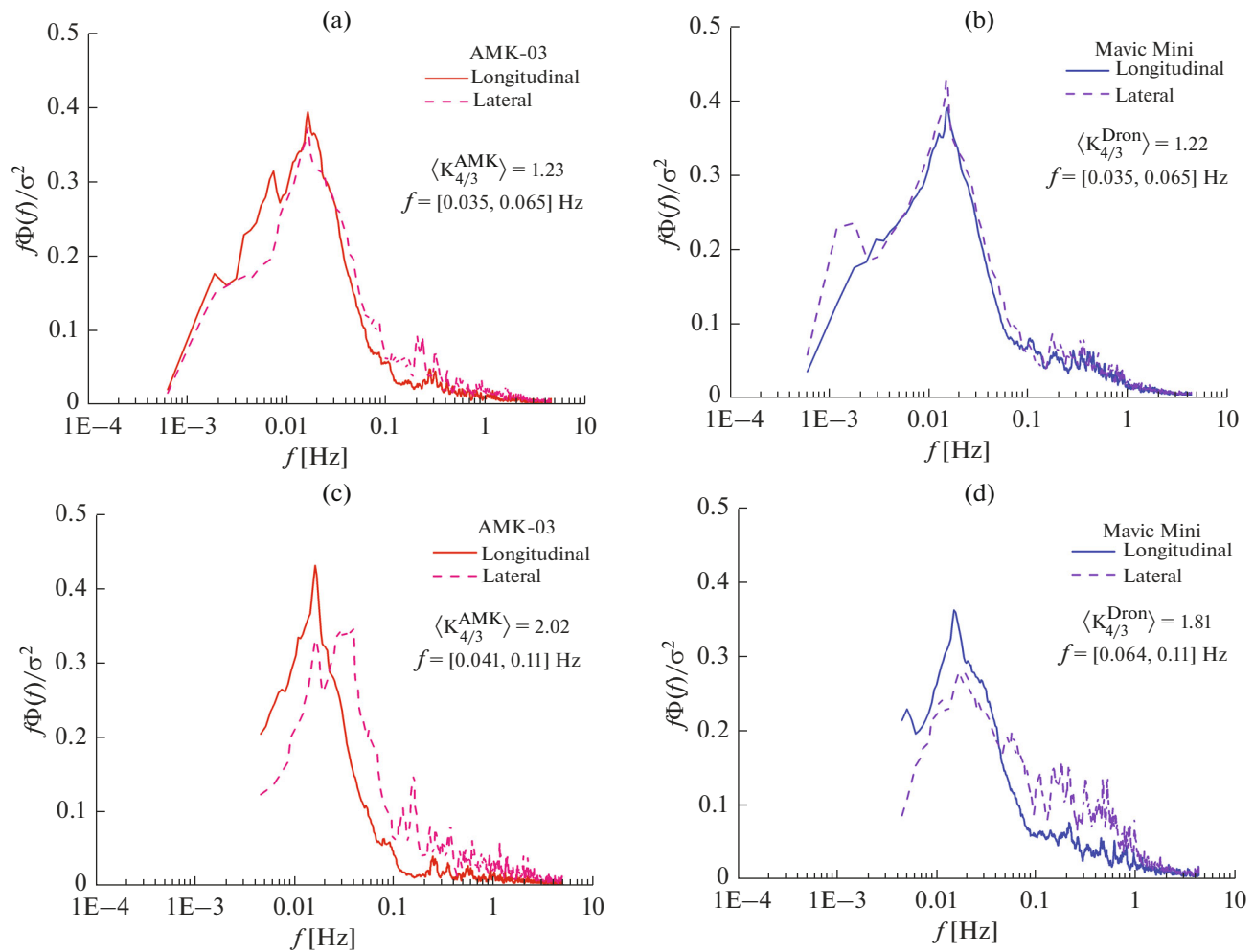


**Fig. 7.** Results of measurements of turbulence spectra on July 24 (a, b) and August 12, 2020 (c, d). Longitudinal and transverse spectra  $f\Phi_u(f)$  and  $f\Phi_v(f)$  calculated according to AMK-03 data (a, c) and according to the DJI Mavic Mini (b, d);  $\sigma^2$  is the normalization factor.

taken on that day using both AMK-03 and the DJI Mavic Mini in the indicated frequency ranges do not coincide with their value for isotropic turbulence. At the same time, there is a good agreement between the values of the coefficient  $K_{4/3}$  between AMK-03 data and the DJI Mavic Mini.

**Table 2.** Integral scales of turbulence

	$L_u$	$L_v$	$L_v/L_u$
June 24, 2020			
AMK-03	13 m	8 m	0.6
DJI Mavic Mini	14 m	9 m	0.6
August 12, 2020			
AMK-03	21 m	12 m	0.6
DJI Mavic Mini	21 m	14 m	0.7

Figure 8 shows the results of a comparison of the spectra of the longitudinal and transverse components for AMK-03 and the DJI Mavic Mini. The comparison results show that, for measurements performed on July 24, 2020, the turbulence spectra of the longitudinal components for two different measurement methods coincide and the same coincidence is observed for the turbulence spectra of the transverse components. In the case of the experiment carried out on August 12, 2020, there is good agreement in the coincidence of the longitudinal turbulence spectra and, for the transverse spectra, there is qualitative agreement.

It is well known that the relative turbulence spectra contain information on the longitudinal and transverse scales of turbulence  $L_u$  and  $L_v$ . To estimate these scales of turbulence, the method of least squares was used; the Karman model (7) and (8) was used as a regression curve.

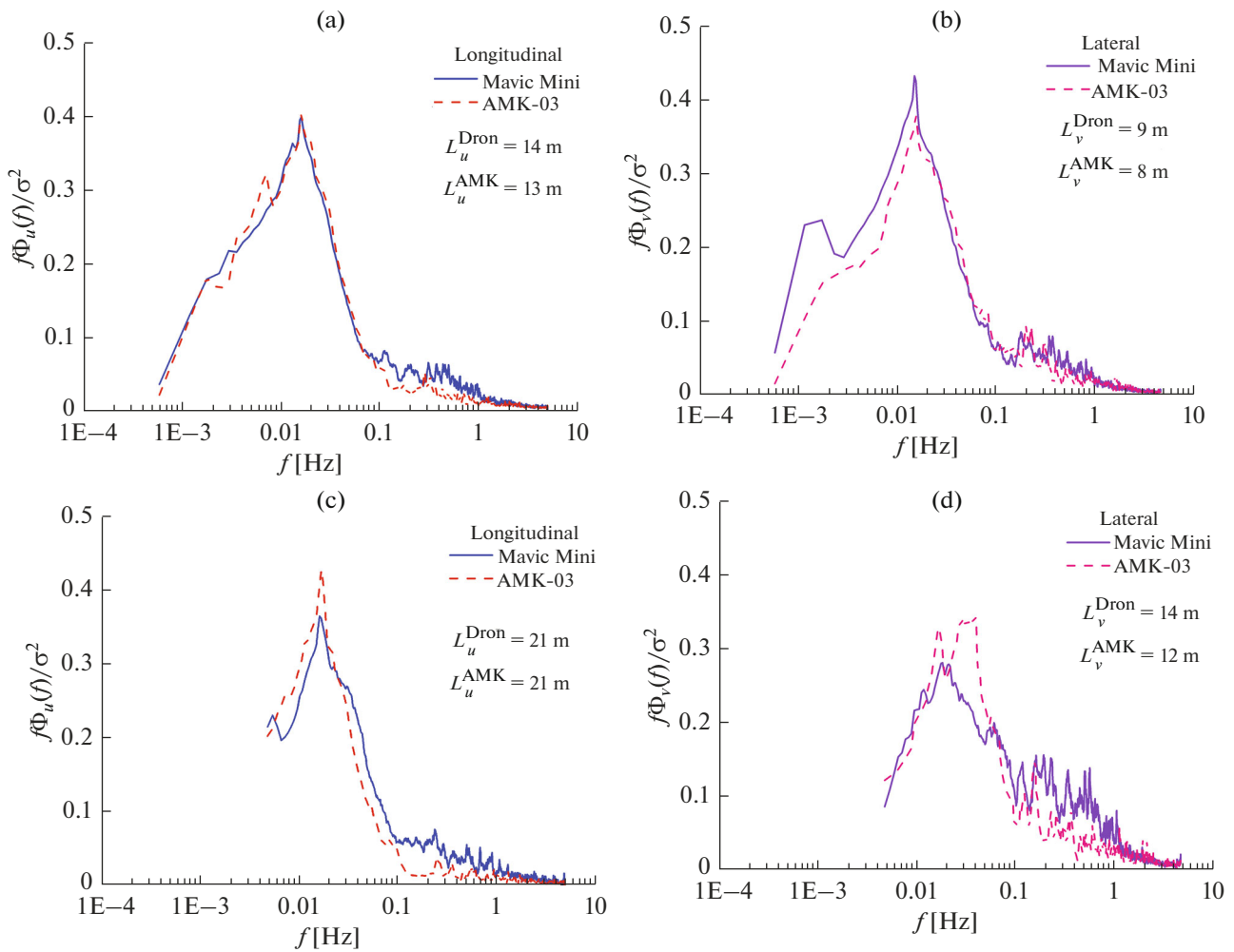


**Fig. 8.** Comparison of longitudinal and transverse turbulence spectra  $f\Phi_u(f)$  and  $f\Phi_v(f)$  calculated according to AMK-03 data and according to the DJI Mavic Mini. Measurement data from July 24 (a, b) and August 12, 2020 (c, d);  $\sigma^2$  is the normalization factor.

The values of the integral scales of turbulence are given in Table 2. It can be seen that the scale of turbulence calculated from the AMK-03 data and the DJI Mavic Mini coincide; condition (9) is also satisfied with good accuracy, which describes the relationship between the longitudinal and transverse scales in an isotropic atmosphere.

### CONCLUSIONS

Based on our studies, the following conclusions can be drawn. This work investigates the spectrum of turbulence in the atmosphere, which was determined on the basis of measurements performed using the DJI Mavic Mini. The obtained turbulence spectra were compared with data from the AMK-03 autonomous meteorological complex, which are objective information on the state of the turbulent atmosphere. The results of two experiments carried out on July 24

and August 12, 2020, at the BEC, Zuev Institute, SB RAS, located on the outskirts of Tomsk are presented.

It was found that the turbulence spectra obtained with AMK-03 and the DJI Mavic Mini, coincide on the whole, and insignificant differences are observed in the high-frequency region of the spectrum starting from  $f \sim 1$  Hz. In the high-frequency region, the turbulence spectrum for the DJI Mavic Mini attenuates slightly with increasing frequency, but faster than in the case of data obtained using AMK-03.

The behavior of smoothed turbulence spectra in the inertial and energy ranges has been studied. For the data obtained on July 24, 2020, the turbulence spectra in the inertial range obey the 5/3 law, and the ratios of the measured turbulence spectra of the transverse and longitudinal velocity components correspond to the isotropic Kolmogorov–Obukhov turbulence  $K_{4/3} = 4/3$ . In the case of measurements car-

ried out on August 12, there was a slight deviation from the 5/3 law, which was recorded both on the basis of measurements obtained with AMK-03 and the DJI Mavic Mini.

To estimate the longitudinal and lateral scales of turbulence, the method of least squares was used and the Karman model was used as a regression curve. Turbulence scales calculated from AMK-03 data and the DJI Mavic Mini coincide, and the condition that describes the relationship between the longitudinal and transverse scales in an isotropic atmosphere is also satisfied with good accuracy.

When analyzing the experimental data, discrepancies in the behavior of the turbulence spectra from their behavior in an isotropic atmosphere are noted and a discrepancy was also observed between the two measurement methods. These discrepancies can be explained as follows. Experimental studies were carried out on a BEC located on a terrain that is not, in the strict sense, a flat and uniform surface. Consequently, one cannot expect an unambiguous coincidence of the AMK-03 and DJI Mavic Mini data with the results of an isotropic atmosphere.

During the experiment, the quadcopter was at a distance of  $\sim 10$  m from AMK-03. Measurements of the integral scales of turbulence have shown that they are of the same order of magnitude as the distance from AMK-03 to the DJI Mavic Mini. Such a ratio of scales and distances means that the wind speed fields at the points where the AMK-03 and the quadcopter are located are partially correlated, so it is necessary to talk about the full correspondence of the measurement data with some degree of caution.

#### APPENDIX

By analogy with formulas (16)–(18), we define the quantities  $\alpha_{\parallel}$  and  $\alpha$  using equations

$$\alpha_{\parallel} = n_x \alpha_x + n_y \alpha_y,$$

$$\alpha = -n_x \alpha_x + n_y \alpha_y,$$

where

$$\alpha_x = -(\langle \varphi \rangle s_{\langle \psi \rangle} + \langle \theta \rangle c_{\langle \psi \rangle}) - (\varphi' s_{\langle \psi \rangle} + \theta' c_{\langle \psi \rangle}),$$

$$\alpha_y = -(\langle \varphi \rangle s_{\langle \psi \rangle} + \langle \theta \rangle c_{\langle \psi \rangle}) - (-\varphi' c_{\langle \psi \rangle} + \theta' s_{\langle \psi \rangle}).$$

The estimates of the longitudinal and transverse components of the wind speed obtained using a quadcopter are defined as

$$\hat{u} = a_{\parallel} \alpha_{\parallel} + b_{\parallel},$$

$$\hat{v} = a_{\perp} \alpha_{\perp} + b_{\perp}.$$

Coefficients  $a_{\parallel}$ ,  $a_{\perp}$ ,  $b_{\parallel}$  and  $b_{\perp}$  are determined from the experiment using formulas

$$a_{\parallel} = \frac{u_{\max} - u_{\min}}{\alpha_{\parallel, \max} - \alpha_{\parallel, \min}},$$

$$a = \frac{v_{\max} - v_{\min}}{\alpha_{\perp, \max} - \alpha_{\perp, \min}},$$

$$b_{\parallel} = \langle u \rangle - a_{\parallel} \langle \alpha_{\parallel} \rangle,$$

$$b_{\perp} = \langle v \rangle - a_{\perp} \langle \alpha_{\perp} \rangle,$$

where  $\langle u \rangle$ ,  $\langle v \rangle$ ,  $u_{\max}$ ,  $v_{\max}$ ,  $u_{\min}$ , and  $v_{\min}$  are average, maximum, and minimum values of the longitudinal and transverse components according to AMK-03 data;  $\langle \alpha_{\parallel} \rangle$ ,  $\langle \alpha_{\perp} \rangle$ ,  $\alpha_{\parallel, \max}$ ,  $\alpha_{\perp, \max}$ ,  $\alpha_{\parallel, \min}$ , and  $\alpha_{\perp, \min}$  are average, maximum, and minimum values of quantities  $\alpha_{\parallel}$  and  $\alpha_{\perp}$ . Based on the data of July 24, 2020  $a_{\parallel} = 0.56$ ,  $b_{\parallel} = 0.16$ ,  $a_{\perp} = 0.50$ , and  $b_{\perp} = 0$ ; however, for August 12, 2020,  $a_{\parallel} = 0.54$ ,  $b_{\parallel} = 0.06$ ,  $a_{\perp} = 0.42$ , and  $b_{\perp} = 0$ .

#### FUNDING

This work was supported by the Russian Foundation for Basic Research, project no. 19-29-06066 MK.

#### REFERENCES

1. L. B. Cornman and W. N. Chan, "Summary of a workshop on integrating weather into unmanned aerial system traffic management," *Bull. Am. Meteorol. Soc.* **98** (10), ES257–ES259 (2017).
2. R. W. Beard and T. W. McLain, *Small Unmanned Aircraft: Theory and Practice* (Princeton Univ. Press, 2012; Tekhnosfera, Moscow, 2015).
3. H. W. Tieleman, "Universality of velocity spectra," *J. Wind Eng. Ind. Aerodyn.* **56** (1), 55–69 (1995).
4. I. A. Repina, M. I. Varentsov, D. G. Chechin, et al., "Unmanned aerial vehicles for studying the atmospheric boundary layer," *Innovatika Ekspert.: Nauchn. Tr.* **2** (30), 20–39 (2020).
5. J. Elston, B. Argrow, M. Stachura, D. Weibel, D. Lawrence, and D. Pope, "Overview of small fixed-wing unmanned aircraft for meteorological sampling," *J. Atmos. Oceanic Technol.* **32** (1), 97–115 (2015).
6. R. T. Palomaki, N. T. Rose, M. Bossche, T. J. Sherman, and S. F. J. De Wekker, "Wind estimation in the lower atmosphere using multirotor aircraft," *J. Atmos. Oceanic Technol.* **34**, 1183–1190 (2017).
7. J. González-Rocha, C. A. Woolsey, and C. Sultan, "Measuring atmospheric winds from quadrotor motion," in *AIAA Atmospheric Flight Mechanics Conference* (Grapevine, Tex., 2017).
8. B. H. Wang, D. B. Wang, Z. A. Ali, B. T. Ting, and H. Wang, "An overview of various kinds of wind effects on unmanned aerial vehicle," *Meas. Control* **52** (7–8), 731–739 (2019).
9. J. González-Rocha, S. F. J. De Wekker, S. D. Ross, and C. A. Woolsey, "Wind profiling in the lower atmosphere from wind-induced perturbations to multirotor UAS," *Sensors* **20**, 1341 (2020).
10. M. Varentsov, V. Stepanenko, I. Repina, A. Artamonov, V. Bogomolov, N. Kuksova, E. Marchuk, A. Pashkin, and A. Varentsov, "Balloons and quadcopters: In-

- tercomparison of two low-cost wind profiling methods,” *Atmosphere* **12**, 380 (2021).
11. J. Reuder and M. O. Jonassen, “Proof of concept for wind turbine wake investigations with the RPAS SUMO,” *Energy Procedia* **94**, 452–461 (2016).
  12. B. D. Reineman, “Development and testing of instrumentation for UAV-based flux measurements within terrestrial and marine atmospheric boundary layers,” *J. Atmos. Oceanic Technol.* **30**, 1295–1319 (2013).
  13. B. D. Reineman, L. Lenain, and W. K. Melville, “The use of ship-launched fixed-wing UAVs for measuring the marine atmospheric boundary layer and ocean surface processes,” *J. Atmos. Oceanic Technol.* **33**, 2029–2052 (2016).
  14. B. B. Balsley, D. A. Lawrence, D. C. Fritts, L. Wang, K. Wan, and J. Werne, “Fine structure, instabilities, and turbulence in the lower atmosphere: High-resolution in situ slant-path measurements with the DataHawk UAV and comparisons with numerical modeling,” *J. Atmos. Oceanic Technol.* **35**, 619–642 (2018).
  15. A. Rautenberg, J. Allgeier, S. Jung, and J. Bange, “Calibration procedure and accuracy of wind and turbulence measurements with five-hole probes on fixed-wing unmanned aircraft in the atmospheric boundary layer and wind turbine wakes,” *Atmosphere* **10**, 124 (2019).
  16. A. Rautenberg, M. Schön, K. Berge, M. Mauz, P. Manz, A. Platis, B. van Kesteren, I. Suomi, S. T. Kral, and J. Bange, “The multi-purpose airborne sensor carrier MASC-3 for wind and turbulence measurements in the atmospheric boundary layer,” *Sensors* **19**, 2292 (2019).
  17. A. P. Shelekhov, F. L. Afanasiev, A. A. Kobzev, and E. A. Shelekhova, “Opportunities to monitor the urban atmospheric turbulence using unmanned aerial system,” *Proc. SPIE: Remote Sens. Technol. Appl. Urban Environ. V* **11535**, 1153506 (2020). <https://doi.org/10.1117/12.2573486>.
  18. A. P. Shelekhov, F. L. Afanasiev, A. A. Kobzev, O. S. Chupina, A. E. Tel'minov, and E. A. Shelekhova, “Spectra of turbulent fluctuations of Euler angles of unmanned aerial vehicles in the altitude holding mode,” *Proc. SPIE: XXVI Int. Symp. Atmos. Ocean Opt., Atmos. Phys.* **11560**, 115605 (2020). <https://doi.org/10.1117/12.2576773>
  19. A. Shelekhov, A. Afanasiev, A. Kobzev, E. Shelekhova, A. Tel'minov, A. Molchunov, and O. Poplevina, “Low-altitude atmospheric turbulence sounding on the basis of unmanned aerial vehicle,” *Preprints* **2020**, 2020090595 (2020). <https://doi.org/10.20944/preprints202009.0595.v1>
  20. A. S. Monin and A. M. Yaglom, *Statistical Fluid Mechanics* (Nauka, Moscow, 1967), Vol. 2 [in Russian].
  21. J. C. Kaimal and J. J. Finnigan, *Atmospheric Boundary Layer Flows. Their Structure and Measurement* (Oxford Univ. Press, Oxford, 1994).
  22. A. A. Azbukin, A. Ya. Bogushevich, V. A. Korolkov, A. A. Tikhomirov, and V. D. Shelevoi, “A field version of the AMK-03 automated ultrasonic meteorological complex,” *Russ. Meteorol. Hydrol.* **34** (2), 133–136 (2009).
  23. A. A. Azbukin, A. Ya. Bogushevich, A. A. Kobzev, et al., “AMK-03 automatic weather stations, their modifications and applications,” *Sens. Syst.* **3** (154), 47–52 (2012).